ACS Catalysis

RESEARCH ARTICLE

pubs.acs.org/acscatalysis

Kinetic and Scanning Transmission Electron Microscopy Investigations on a MCM-41 Supported Cluster Derived Enantioselective Ruthenium Nanocatalyst

Arindam Indra,[†] Mukesh Doble,[‡] Sumit Bhaduri,[*,§] and Goutam Kumar Lahiri[*,†]

[†]Department of Chemistry, Indian Institute of Technology Bombay, Powai, Mumbai-400076, India

[‡]Department of Biotechnology, Indian institute of Technology Madras, Chennai-600036, India

[§]Department of Chemistry, Northwestern University, Evanston, Illinois 60208, United States

Supporting Information

ABSTRACT: The asymmetric hydrogenation of methyl pyruvate to methyl lactate, by cinchonidium functionalized MCM-41 supported $[Ru_4(\mu\text{-}H)_3(CO)_{12}]^-$ as the precatalyst has been studied kinetically and by scanning transmission electron microscopy (STEM). Existence of an induction time and two competitive equilibriums are inferred from the time monitored conversion data. Steady state approximation gives a poor fit, but a kinetic model (Eley−Rideal) consisting of a fast equilibrium between methyl pyruvate and the catalyst, a slow one between the catalyst and dihydrogen, and a rate determining reaction between the latter and methyl pyruvate, accurately simulates the time monitored conversion profiles. The model suggests that on increasing the methyl pyruvate concentration there is a change in the stoichiometry of the equilibrium between the catalyst and the methyl pyruvate. The change in enantioselectivity with time can also be accurately simulated by assuming enantiomeric excess to be proportional to the rate constant for methyl lactate formation. Both kinetic and STEM data strongly suggest that in the fresh catalyst the bare metal cluster framework is retained, and under the catalytic conditions agglomeration of the subnano sized clusters leading to the formation of nanoparticles of ruthenium is a relatively slow process. A hypothetical enantionface selection mechanism consistent with the empirical rate law, previous reports, and other experimental evidence is proposed.

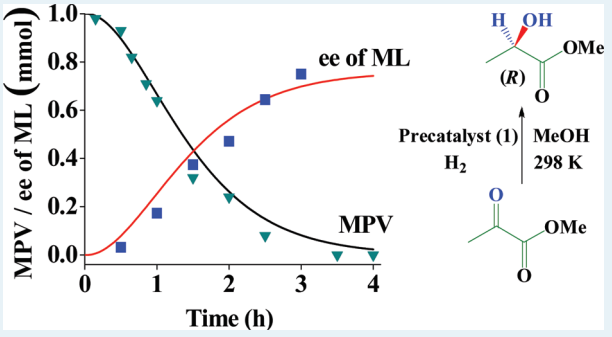

KEYWORDS: ruthenium carbonyl cluster, functionalized MCM-41, hydrogenation catalyst, asymmetric catalysis, nanocatalyst, kinetic model

1. INTRODUCTION

Transition-metal nanoparticles are attractive as catalysts because if controlled, their surface structures often give rise to high chemo-, regio-, stereo-, and enantioselectivities.[1−7] Among the various recently reported preparative methods, the use of metal carbonyl clusters as precursors of nanoparticles of controlled size and shape is one of the promising approaches for obtaining heterogeneous catalysts of high selectivities.[8−11] In our earlier work we reported that anionic carbonyl clusters ion-paired on cross-linked polystyrene or functionalized silica are effective precursors for nanoparticles of unique chemo- and/or enantioselective reactions.[12−17] Among the reactions studied by us, the enantioselective hydrogenation of methyl pyruvate (MPV) to methyl lactate (ML) with cluster derived Pt or Ru nanoparticles, supported on cinchonidium functionalized MCM-41, is of special interest. After the name of its discoverer, the enantioselective hydrogenation of MPV with Pt/Al_2O_3 as the catalyst and cinchona alkaloids as the chiral modifiers is called Orito reaction. In recent years the synthetic potential and mechanistic aspects of the Orito reaction have been extensively investigated and reviewed.[18−24]

At a molecular level the mechanism of enantioselective hydrogenation by the cluster derived catalysts must be different from that of the conventional Orito catalyst for two reasons. First, with conventional Pt/Al_2O_3 catalyst quaternization of the quinuclidine nitrogen leads to complete loss of enantioselectivity, but in the cluster catalysts the chiral agent is the cinchonidium ion.[12,14,24,25] Second, for the Pt/Al_2O_3/cinchona alkaloid catalyst good enantioselectivities and acceptable reaction rates are obtained only after a reductive pretreatment in flowing hydrogen at high temperatures. There is some evidence to show that these pretreatments reduce the size of the platinum particles and help in increasing the enantioselectivity of the reaction.[19,26,27] In contrast for the cluster derived catalysts no such pretreatment is required.

Our initial work was based on catalysts made from anionic platinum carbonyl clusters.[14,15] These catalysts were effective for the asymmetric hydrogenation of MPV to ML, but significant

Received: February 7, 2011
Revised: March 21, 2011
Published: March 23, 2011

enantioselectivities were obtained only at very low turnovers. Subsequently we showed that Orito type reactions are not exclusive attributes of either cinchona alkaloids as the chiral modifiers, or platinum and palladium as the catalytically active metals. The ruthenium cluster based precatalyst **1** where the anionic cluster $[Ru_4(\mu\text{-}H)_3(CO)_{12}]^-$ is supported on chloropropyl cinchonidinium functionalized MCM-41 was found to be far superior to the Pt-cluster derived catalyst, and good enantioselectivity was obtained at much higher turnovers.[28] It may be noted that comparative studies on the enantioselective reductions of a variety ketoesters by bio- and water-soluble chiral ruthenium catalysts have recently been reported.[29] However, for MPV hydrogenation with these ruthenium catalysts the maximum enantioselectivity was ≤12%.

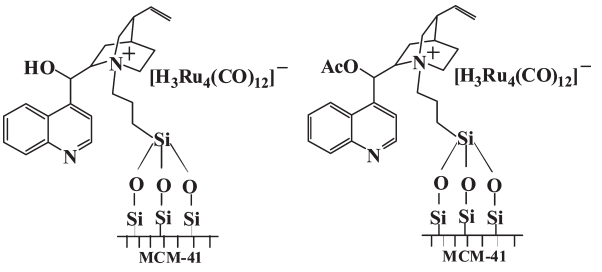

Precatalyst 1 **Precatalyst 2**

The work presented in this paper was undertaken with the primary objective of testing the hypothesis that the active catalytic sites are best approximated as small Ru_n ($n \sim 4$) clusters, and the observed enantioselectivity is largely correlated to the ability of the active sites to retain this structure. To achieve this objective we have carried out detailed kinetic studies. An empirically derived reproducible rate law is a prerequisite for any mechanistic speculation. It may be noted that there are many homogeneous catalytic systems where the spectroscopically observed organometallic species play insignificant or no role at all. In view of this any claim of a single site behavior by a cluster derived heterogeneous catalyst needs to be supported by kinetic data. Although much has been reported on structural characterization of cluster derived nanocatalysts, to the best of our knowledge there have been no detailed kinetic studies on any such system. Here we present kinetic data that is consistent with the proposal that bare metal Ru_4 clusters are the active catalytic species. The kinetic scheme also helps us to compare and contrast some of the mechanistic details of conventional Orito catalysts with that of the cluster derived catalyst. The size and agglomeration behavior of the Ru-clusters in the fresh and used catalysts have been studied by scanning transmission electron microscopy (STEM). The empirical rate expression is found to be consistent with the structural data obtained by STEM. In our earlier work on the Pt-cluster derived catalysts, based on TEM data, the quick loss of enantioselectivity was attributed to rapid agglomeration of the Pt-nanoparticles. Here we present evidence to show that unlike the platinum cluster, the ruthenium cluster does not undergo quick agglomeration.

2. EXPERIMENTAL SECTION

2.1. General Procedures. The general experimental methods, sources of chemicals, and instruments used have been described in our earlier publications.[14,15,28] The STEM experiments were carried out at Northwestern University NUANCE center. Syntheses of $[Ru_4(\mu\text{-}H)_4(CO)_{12}]$[30] and $[Ru_4(\mu\text{-}H)_3(CO)_{12}]^-$ [31−33] were carried out according to the literature reported methods. The 9-O-Acetyl derivative of cinchonidine was prepared according to the literature procedure,[34] and used to functionalize MCM-41. Synthesis and characterization data (IR, XPS, surface area, elemental analysis) and TEM (fresh and used) of **1** has been reported by us in our earlier publication.[28]

2.2. Catalytic Experiments with 1. All the hydrogenation reactions were carried out in an autoclave. Conversions and enantioselectivities of the hydrogenation reactions were monitored by gas chromatography (Shimadzu GC-2014) using a chiral capillary column (SUPELCO-ASTEC-Chiraldex B-DM, fused silica, 50 m × 0.25 mm ×0.12 μm from Sigma-Aldrich).

The catalytic runs in general were carried out at 27 °C in 2 mL of methanol contained in glass vials, with 50 mg catalysts unless specified otherwise. The glass vial was placed in an autoclave, and a hydrogen pressure in the range of 20 to 60 bar was applied with a stirring rate ≥900 rpm. Reactions under five different pressures 20, 30, 40, 50, and 60 bar were studied, and the stirring rate of ≥900 rpm under all these pressures was found to be adequate for giving acceptable (±5%) reproducibility. Any significant change in the catalyst amount required a change in the stirring rate and solvent amount for reproducible data because of change in the mass transfer effects. Consequently variation in catalyst amount was not studied. Each catalytic run was carried out in duplicate, and the data with the variation in conversion and enantioselectivity of ≤5% were used. A calibration graph of weight ratio versus area ratio in chromatographs of synthetic mixtures of methyl pyruvate and methyl lactate showed that linearity was maintained up to a molar ratio of 2.5. Outside this range cyclohexene was used as an external standard.

In kinetic modeling the simulations were performed using MATLAB 7.0 software. The integrations of the differential equations were performed with the function ODE-45, which can be used to solve nonstiff ordinary differential equations with initial conditions. The default relative error tolerance 1×10^{-3} and the default absolute tolerance of 1×10^{-6} for each component were used. A MATLAB function called fminsearch is used to find the minimum of a scalar function of several variables, starting at an initial estimate. This is generally referred to as unconstrained nonlinear optimization. The goodness of fit of the data is given by the MSSE (minimized sum of squares of the errors between model predictions and actual values).

In Model-1 (three parameters, K_1, K_2, k, see Section 3.2) the following two equations are used where $[\mathbf{1}]_0$ and $[\mathbf{1}]_t$ refer to catalyst concentrations initially and at time t.

$$-\frac{d[MPV]}{dt} = \frac{d[ML]}{dt} = \frac{kK_1[\mathbf{1}]_o[H_2][MPV]}{1 + K_1[H_2] + K_2[MPV]}$$

$$[\mathbf{1}]_t + [\mathbf{1}\text{-}2H] + [\mathbf{1}\text{-}MPV] = [\mathbf{1}]_o$$

In Model-2 (three parameters k_1, k_{-1}, k, see Section 3.2) the following equations are used.

$$[\mathbf{1}]_t + [\mathbf{1}\text{-}2H] = [\mathbf{1}]_o$$

$$\frac{d[\mathbf{1}\text{-}2H]}{dt} = k_1[\mathbf{1}]_0[H_2] - k_{-1}[\mathbf{1}\text{-}2H]$$

dx.doi.org/10.1021/cs200058q |ACS Catal. 2011, 1, 511–518

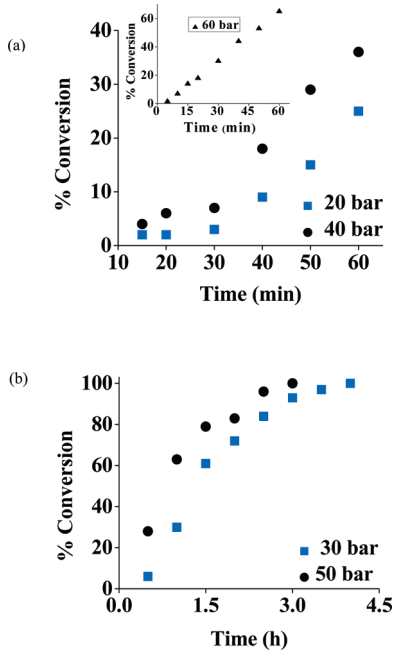

Figure 1. Plot of conversion versus time at (a) 20, 40, and 60 (Inset) bar, (b) 30 and 50 bar with 1 mmol MPV and a MPV:Ru molar ratio of 270.

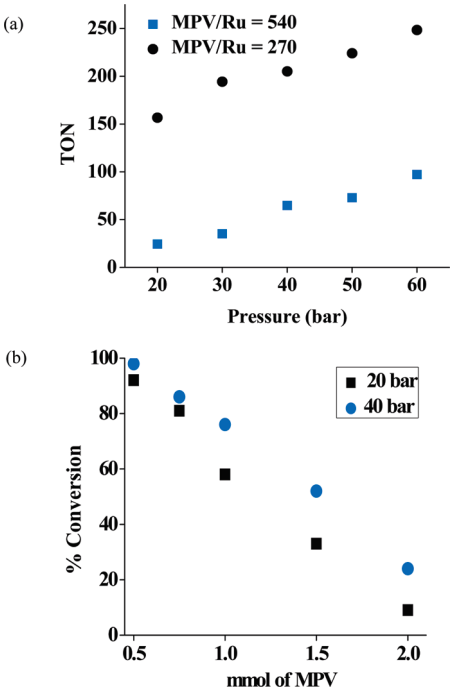

Figure 2. (a) Plot of conversion versus pressure after 2 h reaction at two different MPV/Ru molar ratios. (b) Plot of conversion versus [MPV] after 2 h reaction using 3.7×10^{-3} mmol Ru at 20 and 40 bar.

$$-\frac{\mathrm{d[MPV]}}{\mathrm{d}t} = \frac{\mathrm{d[ML]}}{\mathrm{d}t} = k[\mathbf{1}\text{-2H}][\mathrm{MPV}]$$

In Model-3 (four parameters k_1, k_{-1}, K_2 and k, see Section 3.2) the above two and the following equations are used.

$$[\mathbf{1}]_t + [\mathbf{1}\text{-2H}] + [\mathbf{1}\text{-MPV}] = [\mathbf{1}]_o; \quad [\mathbf{1}\text{-MPV}] = K_2[\mathbf{1}]_t[\mathrm{MPV}]$$

$$[\mathbf{1}]_t = \{[\mathbf{1}]_o - [\mathbf{1}\text{-2H}]\}/\{1 + K_2[\mathrm{MPV}]\}$$

3. RESULTS AND DISCUSSION

3.1. Empirical Rate Expression for the Hydrogenation of Methyl Pyruvate by 1. As mentioned earlier, one of the main motivations for this work was to establish a rate expression by kinetic analysis that simulates the experimental data well. To meet this objective, the effects of varying hydrogen pressure and substrate concentration on conversions of the reaction were studied. From the time monitored conversion data, and conversion at a specific time interval under a specific hydrogen pressure and MPV concentration, the following conclusions may be drawn.

Under pressures 20, 30, and 40 bar, there is clearly an induction time of ~0.5 h after which the hydrogenation sets in (Figure1a, b). However, under higher pressures, 50 and 60 bar, the induction time is shorter (Figure 1a inset, 1b). Our earlier work had shown that under hydrogen pressure, the IR bands for CO in **1** disappear quickly.[28] Two possibilities for the observed induction time may be considered. It is possible that the cluster retains its tetranuclear metal framework but looses the carbonyl ligands, thus becoming co-ordinatively unsaturated, a prerequisite for any catalysis, and the induction time is associated with this process. The second possibility is that the CO groups are lost but with a concomitant change in the nuclearity of the cluster. It must be noted that induction times are also observed in many homogeneous catalytic systems where a change in nuclearity, for example, decomposition of the soluble complex to finely divided metal particles, occurs under the catalytic conditions.[35] As will be seen later kinetic studies taken together with STEM results indicate that out of these two possibilities the first one is more likely.

In control experiments even under relatively low hydrogen pressure, for example, 10 bar, complete loss of CO was observed in less than 5 min. Similarly, passing hydrogen through a suspension of **1** in methanol caused total decarbonylation in ~20 min. The loss of the CO ligands was irreversible, that is, exposure of the decarbonylated material to an atmosphere of carbon monoxide for 24 h did not produce any observable carbonyl bands. As the time taken for CO loss in the control experiments is notably shorter (<5 min at 10 bar) than the observed induction times (~ 30 min at 20 bar), the reaction of the decarbonylated clusters with hydrogen to give the catalytically active intermediate must be relatively slow.

Keeping the MPV concentration constant if pressure is increased, conversion and turnover also increase (Figure 2a). However, from the same plot it is also apparent that at a constant pressure an increase in MPV concentration lowers the relative turnover. As shown in Figure 2b this is further supported by the [MPV] versus conversion plots at two different hydrogen pressures. At 20 bar the turnover numbers (TON) with 0.5 and 2 mmol of MPV after 2 h are 124 and 49, respectively, while at 40 bar the corresponding TON are 132 and 130. These observations indicate competitive equilibriums and inhibition of ML formation by excess MPV. Such inhibition would result if both hydrogen and MPV compete for co-ordination to the catalytically active unsaturated cluster. In other words there are two equilibriums, a productive one between **1** and hydrogen, and

dx.doi.org/10.1021/cs200058q |ACS Catal. 2011, 1, 511–518

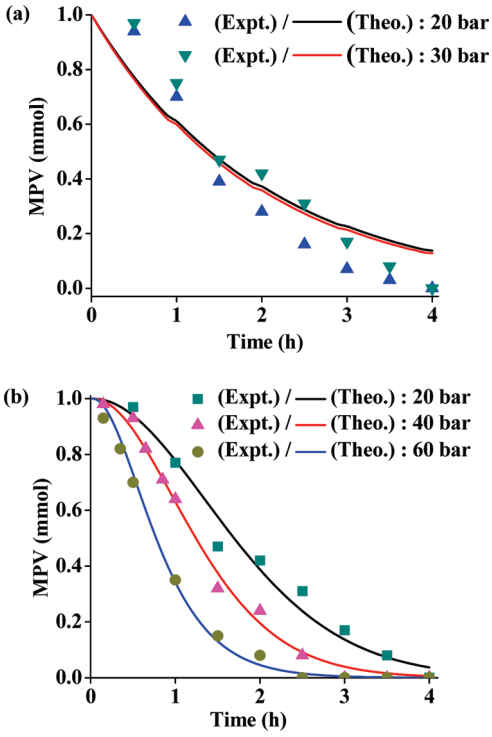

Figure 3. (a) Plot of mmol of MPV versus time (lines are for theoretical value from Model-1 whereas points are from experimental value). (b) Plot of mmol of MPV versus time (lines are for theoretical value from Model-2 whereas points are from experimental value). For both (a) and (b), $[\mathbf{1}]_0 = 3.7 \times 10^{-3}$mmol, $[\mathrm{MPV}]_{t=0}$ =1 mmol.

a nonproductive one between **1** and MPV. It may be noted that similar competitive equilibriums have also been reported for the conventional Pt based Orito catalysts.[36]

Ignoring the induction time mentioned earlier, and based on steady state approximation, a kinetic scheme (see Experimental Model-1) with only three constants, eqs a−c, may therefore be proposed.

$$\mathbf{1} + \mathrm{H_2} \overset{K_1}{\rightleftharpoons} \mathbf{1}\text{-2H} \qquad \text{(a)}$$

$$\mathbf{1} + \mathrm{MPV} \overset{K_2}{\rightleftharpoons} \mathbf{1}\text{-MPV} \qquad \text{(b)}$$

$$\mathbf{1}\text{-2H} + \mathrm{MPV} \overset{k}{\rightarrow} \mathbf{1} + \mathrm{ML} \qquad \text{(c)}$$

In equilibrium a, a catalytically active hydride intermediate **1**-2H is produced. A plausible molecular level formulation of this intermediate is discussed later. However, as shown by equilibrium b in an inhibitory equilibrium MPV competes for the Ru active sites and forms a catalytically nonactive intermediate **1**-MPV. In step c which is the rate determining step, ML is formed from the reaction of **1**-2H and MPV. The model proposed is the classic Eley−Rideal rather than the Langmuir−Hinshelwood model. Models with reactions of adsorbed MPV with adsorbed or free hydrogen to produce ML were considered, but these gave poor fits with experimental data and were not pursued any further. It may be noted that for the conventional Orito reaction, in the only detailed kinetic modeling reported so far, the Langmuir−Hinshelwood−Hougen−Watson formalism has been used.[36] The rate expression for Model-1, that is, reactions a to c, under the steady state approximation is as given below.

$$-\frac{\mathrm{d[MPV]}}{\mathrm{d}t} = \frac{\mathrm{d[ML]}}{\mathrm{d}t} = \frac{kK_1[\mathbf{1}]_o[\mathrm{H_2}][\mathrm{MPV}]}{1 + K_1[\mathrm{H_2}] + K_2[\mathrm{MPV}]}$$

Clearly, based on this kinetic scheme the fit between the simulated concentration profiles and the experimental data in the Time versus [MPV] plot is not good (Figure 3a). The minimized sum of squares of the errors (MSSE) between predicted and experimental values for 30 and 20 bar are 0.017 and 0.03, respectively (Table 1). The poor agreement between predicted and experimental data is expected as this kinetic scheme, while accounting for inhibition by MPV, ignores the observed induction time.

The pressure dependency of the length of the induction time indicates that there is a time delay for the equilibrium to be established between **1** and the catalytically active species **1**-2H. As shown by a′ the slow equilibrium between **1** and **1**-2H can be easily captured in the same kinetic scheme by eliminating the steady state approximation with respect to reaction with hydrogen, and having two rate constants k_1 and k_{-1} for the forward and backward reaction of a.

$$\mathbf{1} + \mathrm{H_2} \underset{k_{-1}}{\overset{k_1}{\rightleftharpoons}} \mathbf{1}\text{-2H} \qquad \text{(a′)}$$

The modified kinetic scheme (Model-2) with three rate constants, k_1, k_{-1}, and k can be used for simulation. In this model, equilibrium b does not have to be considered because in these set of experiments where pressure is varied and induction times are observed, the concentrations of MPV and **1** are kept constant. The modified scheme without the steady state approximation gives much better fit with the experimentally observed data as compared to the unmodified one (Figure 3b). The considerable improvement in the fits is also clear from the MSSE values, which for the 20 bar run reduce by more than an order of magnitude, from 0.03 to 0.0023 (Table 1).

However, to simulate the concentration profiles at different MPV concentrations and to explain the inhibitory effect of increased MPV, equilibrium b must be included in the model. The kinetic scheme with three rate constants k_1, k_{-1}, and k, and one equilibrium constant K_2 (see Experimental Model-3) gives excellent fits between experimental data and simulated concentration profiles at different MPV concentrations (Figure 4a). The highest MMSE of 0.005 and the lowest of 0.0006 are observed for 2.0 and 1.0 mmol of MPV, respectively (Table 1).

It may be noted that a change in the MPV concentration from 0.5 to 2.0 mmol results in a notable increase, from 0.08 to 3.4, in the corresponding K_2 value (Table 1). Such a large change in the value of K_2 is expected if and only if with increased MPV concentration, there is a concomitant change in the stoichiometry of the equilibrium. Assuming that each catalytic site retains the tetrahedral Ru_4 cluster framework of the original cluster, with high MPV concentration co-ordination by more than one MPV molecule to each of these sites is likely. In other words with increased MPV concentration, in addition to **1**-[MPV], adducts such as **1**-$[\mathrm{MPV}]_n$ (n = 2 and/or 3, 4) may also be formed. The kinetic data therefore rules out dissociation of the cluster to uniformly distributed mononuclear sites, and it is reasonable to propose that during catalysis the decarbonylated clusters retain their molecular identities. It may be noted that MPV adsorption on a clean Pd (111) surface in two different orientations, planar and perpendicular to the surface depending on the coverage, has

dx.doi.org/10.1021/cs200058q |ACS Catal. 2011, 1, 511–518

Table 1. Optimized Kinetic Parameters

	pressure (bar)	MPV (mmol)	k (bar^{-1} h^{-1})	K_1	K_2 (mmol^{-1})	MSSE ($\times 10^3$)
Model 1	30	1	0.61	0.25	0.14	17
	20		0.58	0.45	0.3	30
	pressure (bar)	MPV (mmol)	k (bar^{-1} h^{-1})	k_1 ($\times 10^4$) (bar^{-1} h^{-1})	k_{-1} ($\times 10^4$) (h^{-1})	K_2 (mmol^{-1})	MSSE ($\times 10^3$)
Model 2	20			6.6			2.3
	40	1	29	6.5	7	0.12	0.9
	60			13			0.35
Model 3		0.5	27	6.5	7	0.08	1.3
	40	1.0	29	6.5	7	0.12	0.6
		2.0	29	6.5	7	3.4	5
	pressure (bar)	MPV (mmol)	k' (h^{-1})	k_1 ($\times 10^4$) (bar^{-1} h^{-1})	k_{-1} ($\times 10^4$) (h^{-1})	K_2 (mmol^{-1})	MSSE ($\times 10^3$)
Model 3	20	1	0.59	6.6	7	0.12	1.1
	40		0.61	6.5	7	0.12	0.88
	60		0.61	13	7	0.12	0.77

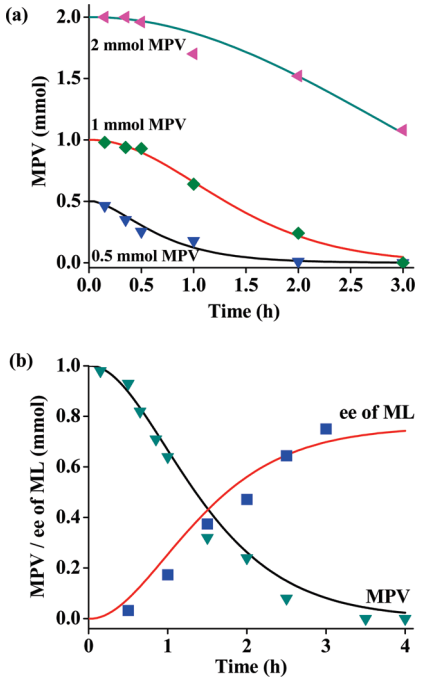

Figure 4. (a) Plot of mmol of MPV versus time (lines are for theoretical values from Model-3 whereas points are from experimental values). (b) Plot of mmol of MPV and ee of ML converted to mmol versus time (lines are for theoretical value from Model-3 and points are experimental values).

recently been reported.[37] Similar modes of interaction by MPV with well-defined uniform crystal faces of the bare Ru_4-cluster may also give rise to the observed change in K_2. The overall rate expression therefore indicates a transition state that involves Ru_4 clusters, adsorbed hydrogen, and MPV.

Finally, it may be noted that most of the reported mechanistic studies on the conventional Orito catalyst have been carried out in a batch reactor, and the analyses are based on steady state approximations.[36,38] With our catalyst we could have ignored the induction times, measured the initial rates after the induction time, and fitted the rate expression of Model-3 assuming $[\mathbf{1}] \approx [\mathbf{1}]_0$. This, however, is clearly an unsatisfactory methodology as it leaves the origin of the induction time, and more importantly the notable increase in enantioselectivity with time unexplained (see later).

3.2. Simulation of Enantioselectivity and Probable Mechanisms for Enantioface Selection. In our earlier publication[28] we had reported that under high pressures ($\geq$50 bar) the maximum ee (enantiomeric excess) was reached at a conversion level $\geq$85% after which there was a reduction in ee. At other pressures we had noted a remarkable change in ee at low conversion levels, the ee's were noticeably low at low conversions ($\leq$30%), but increased as the reaction progressed. The hydrogen pressure of 40 bar was found to be the optimum pressure; at which there was a progressive increase in ee and at full conversion the maximum ee ~75% with *R*-methyl lactate as the major isomer was obtained.[28]

The much expanded database of the present work confirms all our earlier observations. It also shows that the increase in ee's with increasing conversion is $\geq$20%, and could be as high as ~35%. Similar observations have also been made for the conventional Orito system where the difference between measured ee at a specific reaction time and the actual incremental ee being produced covers a wide range, ~ 3−30%.[36,38] A critical test for the proposed Eley−Rideal model with the unsteady state equilibrium (Model-3) is therefore to see to what extent it could reproduce this remarkable increase in ee's with increasing conversions. Indeed as pointed out by others, any mechanistic proposal for the conventional Orito system must not assume that ee is independent of conversion, especially at relatively low conversion levels.[38] As mentioned earlier, in the context of our catalytic system one of the major limitations of any kinetic analysis based on initial rate data and steady state approximation would have been the failure to address this point adequately.

As mentioned earlier there is no kinetic evidence to suggest that adsorption of MPV is a prerequisite for its reaction with hydrogen to give ML. The equilibrium between **1** and MPV involving a specific enantioface of the latter cannot therefore be the enantioselection step. To a first approximation the rate constant "k" for the product formation step c is the sum of two rate constants k_R and k_S corresponding to the R and S isomers of ML. As the observed ee is directly proportional to $k_R - k_S$, the molar concentration of the optically active product at a given

dx.doi.org/10.1021/cs200058q |*ACS Catal.* 2011, 1, 511–518

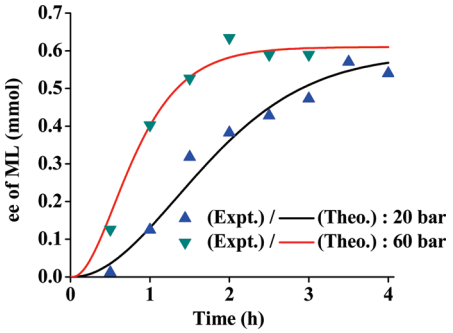

Figure 5. Plot of ee of ML in mmol versus time at 20 and 60 bar (line is for theoretical values from Model-3 and points are experimental values).

time is given by d where k' is $(k_R - k_S)/k$.

$$k'[\mathrm{ML}] = R\text{-}[\mathrm{ML}] - S\text{-}[\mathrm{ML}] \qquad (\mathrm{d})$$

Indeed, the match between the experimentally observed time monitored ee and the theoretically predicted values by this simple model is excellent (Figure 4b and Figure 5). At all the three pressures the model captures the increase in ee with conversion well with MSSEs ~ 0.0008−0.001. The value of k', ~0.6 (Table 1), indicates that k_R is about 4 times faster than k_S. Assuming that k_R and k_S have the same pre-exponential factor, simple calculations show that the difference in free energy of activation $\Delta(\Delta G^{\ddagger})$ for $k_R/\ k_S = 4$, is ≤1 kcal.

In conventional Orito catalysts the solvent has been shown to exert a considerable influence on ee which in turn has been shown to be related to the solubility of the alkaloid in a given solvent, as well as its adsorption mode on to the metal.[39,40] In view of these results, the effects of different solvents and temperatures on conversion and enantioselectivity of the cluster catalyzed reaction have also been studied (Table 2, Entries 1−4). Alcoholic solvents are found to give better enantioselectivities than the others, and among the alcoholic solvents methanol is the best. A change in the solvent has more of an effect on the enantioslectivity of the catalyst than on conversion. Thus, changing the solvent from methanol to cyclohexane results in a drop in enantioselectivity of ~50%, but only ~6% in conversion. An increase in temperature expectedly increases the reaction rates; at 273, 300, and 333 K conversions in 2 h are 26, 76 and 100%, respectively. However, at the lower temperature no significant improvement in enantioselectivity is observed.

On the basis of the empirically derived rate expression, we may propose the following mechanism for the formation of both *R*- and *S*- enantiomers of ML. Under hydrogen pressure the carbonyl groups of $[H_3Ru_4(CO)_{12}]^-$ are lost and the time taken for this is reflected in the induction time. Hydrogen and MPV compete for the coordinatively unsaturated Ru_4 clusters, or subnanosized Ru particles with uniform crystal faces. Of the two possibilities we prefer the former for the following reasons. A nude tetrahedral Ru_4 cluster can provide uniform 111 crystal planes, and the 111 faces of nano-Pt in Orito catalysis have been shown to give higher enantioselectivity than the other crystal faces.[19] Also, there are several reports where Rh_4 clusters have been shown to be the dominant catalytically active species in hydrogen generation from H_3BNH_3.[40−42] These findings are indicative that weakly ligated tetranuclear tetrahedral clusters are relatively stable and catalytically active. Thus **1**-2H is tentatively

Table 2. Effect of Solvent, Temperature, and Acylation of Cinchonidine Hydroxyl on Conversion and ee[a]

entry	catalyst	conversion (ee)%
1	**1**	100 (75)
2[b]	**1**	97 (68), 96 (63), 94 (54),
3[c]	**1**	96 (42), 96 (34), 94 (27)
4[d]	**1**	26 (54), 76 (62), 100 (46)
5[e]	**1**	36 (48)
6	**2**	100 (24)
7	**3**	no conversion

[a] 1 mmol substrate, 5 mL of methanol, 300 K, 40 bar H_2, 50 mg of catalyst, 180 min unless specified otherwise. [b] EtOH, ^{i}PrOH, ^{t}BuOH, respectively. [c] Dichloromethane, tetrahydrofuran, cyclohexane, respectively. [d] 120 min at 273, 300, and 333 K, respectively. [e] 300K, 60 min.

formulated as $[Ru_4H_n]^-$ $(n \geq 3)$ ion-paired with cinchonidium cations on the MCM-41 surface. Excluding the hydrides, the coordination sphere of the cluster probably consists of a weakly ligated framework oxygen atom of MCM-41 and solvent molecules. The rate expression clearly indicates a transition state that involves Ru_4 clusters, hydride ligands, and MPV in the rate determining step. Formation of ML from MPV requires transfer of two hydrogen atoms, of which the transfer of the hydrogen atom to the carbon atom of the carbonyl functionality is the enantioselection step. The rate limiting step is therefore proposed to be slow co-ordination by MPV to $[Ru_4H_n]^-$ followed by fast hydrogen atom transfers.

Two observations related to the enantioselection behaviors of conventional Orito catalysts (Pt/Al_2O_3 modified with cinchonidine) and **1** may be noted. Both **1** and the Orito catalysts give *R*-methyl lactate as the major enantiomer. An analogue of **1**, made with the 9-O-acetyl derivative of cinchonidine functionalized MCM-41 designated as **2** (Table 2 Entry 6), gives considerably less ee. The higher enantioselectivity of **1** as compared to that of **2** is similar to what has been reported for the Orito reaction. Hydroxy or methoxy substituent at C-9 is known to be optimal, and a reduction in ee or even an inversion in the induction is known to result from a larger substituent. Our attempts to tether cinchonidine rather than cinchonidium ion onto MCM-41 by hydrosilylation has so far been unsuccessful. Also, functionalization of the C-10-C-11 olefinic moiety of cinchonidine with $HS(CH_2)_3Si$ linked to MCM-41 results in a total loss of the catalytic activity presumably because of sulfur poisoning. However, the two similarities mentioned above, that is, *R*-ML the major enantiomer and the drop in enantioselectivity with acetylation of the hydroxyl group, suggest that the enantioselection mechanisms probably share some commonalities.

For the Orito catalyst two possible enantioselection mechanisms have been considered. In both these adsorption of cinchonidine onto the metal through the quinoline ring is proposed. Model density functional theory (DFT) calculations and ATR spectroscopic data on a cichonidine modified platinum surface suggest that multiple conformers of the adsorbed alkaloid are present on the surface, and these are close in energy.[43,44] Enantioselection is thought to result from an interaction between one of these conformers and the adsorbed MPV through hydrogen bonding between the protonated quinuclidine of cinchonidine and the keto-carbonyl group of the ketoester. In the other mechanistic proposal, the formation of a weak substrate-cinchonidine complex in the liquid phase is proposed.[21,38]

In this proposal apart from a donor−acceptor interaction between the nitrogen lone pair of quinuclidine and the keto group of MPV, $\pi-\pi$ interaction between the quinoline ring and the ketoester functionality is also invoked.

In **1** the quinoline ring is free, and the chiral agent is the cinchonidium cation anchored to MCM-41 by a chloropropyl spacer group.[14,15,28] The involvement of the nitrogen lone pair of quinuclidine in hydrogen bonding or in any donor−acceptor type interaction may therefore be ruled out. A more relevant parallel may be found in the solution NMR (NOESY) studies of protonated cinchonidine and the corresponding calculated minimum energy structures.[45] Interestingly the conjugate base anions Cl^- and F^- are found to play an active role in stabilizing the resulting structures, and one of the two lowest-energy conformations is found to be a non-hydrogen bonded ion pair conformation in which the conjugate base anion interacts with the electrostatically positive plane of the aromatic system. In **1**-[2H] too, $[Ru_4H_n]^-$ may form a similar ion pair with the chloropropyl cinchonidium cation thereby ensuring a chiral environment close to the Ru atoms. Thus we propose that the chiral interaction between the cinchonidium cation and MPV is primarily through the quinoline ring and the ketoester functionality.

The large solvent effect on enantioselectivities of the reaction discussed earlier is consistent with this hypothesis. The energies of different possible conformers of the cinchonidium cation are expected to be very close, and the relative stabilization of any particular conformer must be highly sensitive to the nature and the extent of solvation. Also, if as proposed the chiral interaction is through the quinoline ring and the ketoester functionality, a change from alcoholic solvents to nonalcoholic ones may be expected to show a notable influence on ee. This is because in reactions carried out in alcoholic solvents with conventional Orito catalysts, the formation of ketal and hemiketal in small quantities have been reported. With the cluster derived catalysts, formation of such products to a detectable extent has not been observed. However, an interaction between the hydroxyl functionality of the alcoholic solvent and MPV, a prerequisite equilibrium reaction for hemiketal or ketal formation, is certainly likely. This in turn is expected to have an effect on the chiral interaction between the quinoline ring and the ketoester functionality thereby affecting the observed ee.

3.3. STEM (HAADF) Studies. In our earlier work with platinum cluster-derived catalysts, extensive aggregation leading to the formation of large metal particles were observed. This was proposed to be the main reason behind the rapid loss in enantioselectivity.[14,15] A hydrogen pressure dependent rapid aggregation step accompanied by loss in enantioselectivity was therefore included in the kinetic model that was proposed on a limited database. In contrast, inclusion of such a step is not at all necessary for **1** as the agreements between experimental and theoretical points are already very good. However, as mentioned earlier, at higher pressure especially at 60 bar there is a reduction in ee (∼15%) after a conversion level of ∼90%. This probably indicates that aggregation of the $[Ru_4H_n]^-$ clusters does occur but at a rate that is much slower than that of the Pt-clusters.

In our earlier work TEM images of freshly prepared **1** and images after its use in a catalytic run were reported. The hexagonal array of MCM-41 was found to be retained in both fresh and used catalyst.[28] As no distinct Ru-particles could be observed, we concluded that in the fresh catalyst the clusters remain intact, and the $[H_3Ru_4(CO)_{12}]^-$ anions are located in the pores of MCM-41. We also conjectured that if in the used catalyst Ru-aggregation leading to larger particles did take place, the size of such particles must have been sufficiently small and hence not observed. However, the TEM used by us was of relatively low resolution, and TEM is also known to modify small metal clusters on supports during the imaging process. Indeed it is because of the latter reason, high resolution, high angle annular dark field (HAADF) with Z-contrast, STEM has emerged as the technique of choice for studying the structure of metal clusters synthesized via molecular precursors.[46−48] The HAADF-STEM data reported below provide experimental evidence for molecular clusters in the fresh catalyst and for slow agglomeration under the catalytic conditions.

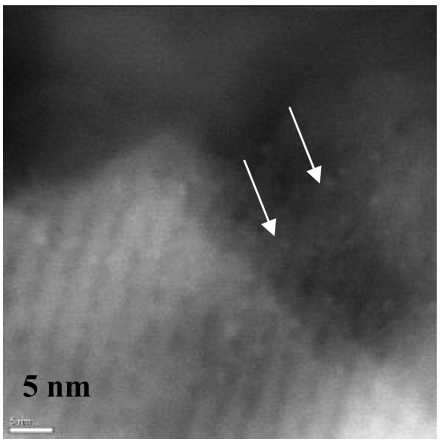

Figure 6. HAADF-STEM image of fresh catalyst **1** at 5 nm resolution. Z-contrast shows uniform dispersion of subnanometer Ru cluster, ∼ 0.5 nm.

STEM images of **1** before its use as a catalyst show MCM-41 arrays and uniform dispersion of subnanometer Ru clusters (Figure 6). It is interesting to note that on the basis of an atomic radius of 0.13 nm for ruthenium, the size (∼ 0.5 nm) of the nanoparticles fits well with the calculated value for "Ru_4". The elemental compositions of the examined areas have been analyzed by energy dispersive X-ray (EDX) and show all the expected signals (Figure S4 in Supporting Information). The Z-contrast of **1** after its use as a catalyst (TON ∼ 270) shows uniform but slightly coarser Ru clusters of ≤1 nm size (Supporting Information). As reported in our earlier publication, with the recycled catalyst there is a decrease in conversion and ee. In view of the observed structural change, this drop in activity and enantioselectivity is expected. After long and repeated use (TON ∼ 510), there is a more pronounced change in the size and distribution of the nanoparticles, when localized, agglomerated clusters ∼2−3 nm in size are seen. As mentioned earlier, the agglomeration process for platinum cluster derived catalysts is much faster; after only a few turnovers, platinum crystallites ≥5 nm are seen at the grain boundaries of MCM-41. The structural data on **1** therefore is consistent with our kinetic model. A pressure dependent cluster aggregation step with resultant loss of enantioselectivity of the catalytic sites need not be included in the model as it does not significantly improve its accuracy.

4. CONCLUSIONS

We have presented a kinetic model (Eley−Rideal) for the enantioselective hydrogenation of MPV where **1** is used as the precatalyst. The model consists of a steady state equilibrium

between MPV and **1**, a slow equilibrium (two rate constants) between hydrogen and **1** and a rate constant for the product formation step. The model simulates well the observed induction time and the inhibitory effect of increased MPV concentration at constant pressure. It is consistent with the hypothesis that weakly ligated tetra-metal hydride clusters are the catalytically active intermediates. Assuming that the observed enantioselectivity is proportional to the rate constant for ML formation, the model simulates the change in enantioselectivity at different pressures well. The STEM data indicate that in the fresh catalyst the bare metal cluster framework is retained, and under the catalytic conditions agglomeration of the clusters is a slow process. A hypothetical enantionface selection mechanism consistent with the kinetic model, STEM, and previous reports is proposed.

■ ASSOCIATED CONTENT

Supporting Information. HAADF-STEM image of fresh and used catalyst **1**, EDX spectra of **1**. This material is available free of charge via the Internet at http://pubs.acs.org.

■ AUTHOR INFORMATION

Corresponding Author

*E-mail: lahiri@chem.iitb.ac.in (G.K.L.). Phone: +91 22 25767159 (G.K.L.). Fax: +91 22 25723480 (G.K.L.).

■ ACKNOWLEDGMENT

We thank Professor V. Dravid of Northwestern University, U.S.A. for arranging the STEM experiments. Financial assistance from Reliance Industries Limited, Mumbai, Council of Scientific and Industrial Research (CSIR), India, is gratefully acknowledged.

■ REFERENCES

(1) Somorjai, G. A.; Li, Y. *Top. Catal.* **2010**, *53*, 832–847.
(2) Vinod, C. P. *Catal. Today* **2010**, *154*, 113–117.
(3) Schmidt, E.; Kleist, W.; Krumeich, F.; Mallat, T.; Baiker, A. *Chem.—Eur. J.* **2010**, *16*, 2181–2192.
(4) Witham, C. A.; Huang, W.; Tsung, C.-K. ; Kuhn, J. N.; Somorjai, G. A.; Toste, F. D. *Nat. Chem.* **2010**, *2*, 36–41.
(5) Mostafa, S.; Behafarid, F.; Croy, J. R.; Ono, L. K.; Li, L.; Yang, J. C.; Frenkel, A. I.; Cuenya, B. R. *J. Am. Chem. Soc.* **2010**, *132*, 15714–15719.
(6) Zaera, F. *Acc. Chem. Res.* **2009**, *42*, 1152–1160.
(7) Maity, P.; Gopinath, C. S.; Bhaduri, S.; Lahiri, G. K. *Green Chem.* **2009**, *11*, 554–561.
(8) Kulkarni, A.; Lobo-Lapidus, R. J.; Gates, B. C. *Chem. Commun.* **2010**, *46*, 5997–6015.
(9) Thomas, J. M.; Raja, R. *Top. Catal.* **2010**, *53*, 848–858.
(10) Adams, R. D.; Boswell, E. M.; Captain, B.; Hungria, A. B.; Midgley, P. A.; Raja, R.; Thomas, J. M. *Angew. Chem., Int. Ed.* **2007**, *46*, 8182–8185.
(11) Thomas, J. M.; Raja, R.; Lewis, D. W. *Angew. Chem., Int. Ed.* **2005**, *44*, 6456–6482.
(12) Bhaduri, S.; Darshane, V. S.; Sharma, K.; Mukesh, D. *J. Chem. Soc., Chem.Commun.* **1992**, 1738–1740.
(13) Paul, H.; Bhaduri, S.; Lahiri, G. K. *Organometallics* **2003**, *22*, 3019–3021.
(14) Basu, S.; Paul, H.; Gopinath, C. S.; Bhaduri, S.; Lahiri, G. K. *J. Catal.* **2005**, *229*, 298–302.
(15) Basu, S.; Mapa, M.; Gopinath, C. S.; Mukesh, D.; Bhaduri, S.; Lahiri, G. K. *J. Catal.* **2006**, *239*, 154–161.
(16) Maity, P.; Basu, S.; Bhaduri, S.; Lahiri, G. K. *Adv. Synth. Catal.* **2007**, *349*, 1955–1962.
(17) Maity, P.; Basu, S.; Bhaduri, S.; Lahiri, G. K. *J. Mol. Catal. A: Chem.* **2007**, *270*, 117–122.
(18) Szollosi, G.; Cserenyi, S.; Bucsi, I.; Bartok, T.; Fulop, F.; Bartok, M. *Appl. Catal., A* **2010**, *382*, 263–271.
(19) Schmidt, E.; Vargas, A.; Mallat, T.; Baiker, A. *J. Am. Chem. Soc.* **2009**, *131*, 12358–12367.
(20) Mink, L.; Ma, Z.; Olsen, R. A.; James, J. N.; Sholl, D. S.; Mueller, L. J.; Zaera, F. *Top. Catal.* **2008**, *48*, 120–127.
(21) Talas, E.; Margitfalvi, J. L. *Catal. Commun.* **2008**, *9*, 984–989.
(22) Mallat, T.; Orglmeister, E.; Baiker, A. *Chem. Rev.* **2007**, *107*, 4863–4890.
(23) Blaser, H.-U.; Studer, M. *Acc. Chem. Res.* **2007**, *40*, 1348–1356.
(24) Burgi, T.; Baiker, A. *Acc. Chem. Res.* **2004**, *37*, 909–917.
(25) Blaser, H. U.; Jalett, H. P.; Monti, D. M.; Baiker, A.; Wehrli, J. T. *Stud. Surf. Sci. Catal.* **1991**, *67*, 147–155.
(26) Orito, Y.; Imai, S.; Niwa, S. *J. Chem. Soc. Jpn.* **1979**, 1118–1120.
(27) Mallat, T.; Frauchiger, S.; Kooyman, P. J.; Schurch, M.; Baiker, A. *Catal. Lett.* **1999**, *63*, 121–126.
(28) Indra, A.; Basu, S.; Kulkarni, D. G.; Gopinath, C. S.; Bhaduri, S.; Lahiri, G. K. *Appl. Catal., A* **2008**, *344*, 124–130.
(29) Zeror, S.; Collin, J.; Fiaud, J.; Zouioueche, L. A. *Tetrahedron Asymm.* **2010**, *21*, 1211–1215.
(30) Knox, S. A. R.; Koepke, J. W.; Andrews, M. A.; Kaesz, H. D. *J. Am. Chem. Soc.* **1975**, *97*, 3942–3947.
(31) Bruce, M. I.; Jensen, C. M.; Jones, N. L. *Inorg. Synth.* **1990**, *28*, 216–222.
(32) Bruce, M. I.; Jensen, C. M.; Jones, N. L. *Inorg. Synth.* **1989**, *26*, 262–263.
(33) Koepke, J. W.; Johnson, J. R.; Knox, S. A. R.; Kaesz, H. D. *J. Am. Chem. Soc.* **1975**, *97*, 3947–3952.
(34) Blaser, H.-U.; Jalett, H. P.; Lottenbach, W.; Studer, M. *J. Am. Chem. Soc.* **2000**, *122*, 12675–12682.
(35) Widegren, J. A.; Finke, R. G. *J. Mol. Catal. A: Chem.* **2003**, *198*, 317–341.
(36) Blaser, H.-U.; Jalett, H.-P. ; Garland, M.; Studer, M.; Thies, H.; Tijani, A. W. *J. Catal.* **1998**, *173*, 282–294.
(37) Burkholder, L.; Tysoe, W. T. *J. Phys. Chem. C* **2009**, *113*, 15298–15306.
(38) Margitfalvi, J. L.; Hegedus, M.; Tfirst, E. *Tetrahedron Asymm.* **1996**, *7*, 571–580.
(39) Zaera, F. *J. Phys. Chem. C* **2008**, *112*, 16196–16203.
(40) Ma, Z.; Lee, I.; Zaera, F. *J. Am. Chem. Soc.* **2007**, *129*, 16083–16090.
(41) Jaska, C. A.; Manners, I. *J. Am. Chem. Soc.* **2004**, *126*, 9776–9785.
(42) Rousseau, R.; Schenter, G. K.; Fulton, J. L.; Linehan, J. C.; Engelhard, M. H.; Autrey, T. *J. Am. Chem. Soc.* **2009**, *131*, 10516–10524.
(43) Vargas, A.; Ferri, D.; Bonalumi, N.; Mallat, T.; Baiker, A. *Angew. Chem., Int. Ed.* **2007**, *46*, 3905–3908.
(44) Vargas, A.; Baiker, A. *J. Catal.* **2006**, *239*, 220–226.
(45) Olsen, R. A.; Borchardt, D.; Mink, L.; Agarwal, A.; Mueller, L. J.; Zaera, F. *J. Am. Chem. Soc.* **2006**, *128*, 15594–15595.
(46) Yang, F.; Trufan, E.; Adams, R. D.; Goodman, D. W. *J. Phys. Chem. C* **2008**, *112*, 14233–14235.
(47) Vang, R. T.; Lauritsen, J. V.; Lagsgaard, E.; Besenbacher, F. *Chem. Soc. Rev.* **2008**, *37*, 2191–2203.
(48) Ward, E. P. W.; Arslan, I.; Bleloch, A.; Thomas, J. M.; Midgley, P. A. *J. Phys. Conf. Ser.* **2006**, *26*, 207–210.